Heterocyclic Letters
Vol. 14| No.1|181-201 |Nov-Jan|2024
ISSN : (print) 2231–3087 / (online) 2230-9632
CODEN: HLEEAI
http://heteroletters.org

SYNTHESIS, CHARACTERIZATION AND APPLICATION STUDIES OF TiO_2-PHOSPHOTUNGSTIC ACID NANOCOMPOSITS PREPARED BY BLENDING METHOD

Praveendaniel M[1], Rajesh Anantha Selvan P[2], Paramanantha Swami Doss D[3]

[1]Research scholar Reg.No-20111272031005, Department of Chemistry, St. John's College, Palayamkottai, Tirunelveli, Tamil Nadu, Affiliated to Manonmaniam Sundaranar University, Tirunelveli. India
[2]Assistant Professor Department of Chemistry, St. John's College, Palayamkottai, Tirunelveli, Tamil Nadu, Affiliated to Manonmaniam Sundaranar University, Tirunelveli. India
[3]Assistant Professor Department of Zoology, St. John's College, Palayamkottai, Tirunelveli, Tamil Nadu, Affiliated to Manonmaniam Sundaranar University, Tirunelveli. India
Corresponding Authur Email: ***rajesh.chem@stjohnscollege.edu.in***

ABSTRACT:
TiO_2-PTA nanocomposites were synthesized by blending method and characterized by UV-visible, FT-IR, XRD, EDX, and SEM. The results showed that there is a strong interaction between TiO_2 and PTA, with a decreased crystallite size and uniformly distributed dopant. The nanocomposites showed excellent photocatalytic activity, with a degradation efficiency of 99.64%. The electrical conductivities of the nanocomposites increased with increasing temperature, and the dielectric constants were positive. The nanocomposites also had significant antimicrobial activity against Streptococcus pyogenes. These results suggest that the TiO_2-PTA nanocomposites have promising properties for applications in many different fields.

KEY WORDS: TiO_2, PTA, nanocomposites, photocatalytic activity, electrical conductivity, antimicrobial activity.

INTRODUCTION:

Nanocomposites are composed of very small elements, typically well below the nano-scale (10^{-9} m), and are fabricated using advanced technologies like carbon nanotubes, nanofibers, nanowires, and other similar methods[1]. They can be used to improve the properties of materials such as strength, light weight, flexibility, photosensing nature and electical conductivity, making them useful in a variety of different applications. Additionally, nanocomposites offer a cost-effective and environmentally friendly[2].

TiO_2 nanocomposites are a new class of materials combining nanomaterials with traditional materials with one or more dimensions ranging between 1 to 100 nanometres. TiO_2

nanocomposites are created by combining TiO_2 nanoparticles with traditional organic or inorganic materials. This combination produces enhanced properties like improved electrical, optical, thermal, and mechanical properties, which are superior to either material alone in specific applications[3].

Phosphotungstic acid (PTA) nanocomposites are a type of material that is made up of PTA molecules and other materials, such as metal oxides or polymers[4]. These nanocomposites have a number of properties that make them useful for a variety of applications, including catalysis, sensing, and energy storage. PTA is a heteropoly acid, which means that it is a complex molecule that contains metal ions and oxygen atoms. PTA molecules are typically arranged in a cage-like structure, with the metal ions at the center of the cage and the oxygen atoms forming the cage walls.

TiO_2 doped with PTA nanocomposites are materials that exhibit excellent photocatalytic[5], antimicrobial, and electrical properties. Recently, there have been many research efforts towards developing TiO_2 doped with PTA nanocomposites by blending methods. The blending technique is a method that involves combining two or more nanomaterials to create a single nanocomposite. This method helps to improve the properties of the nanocomposite material by improving the solubility, packing, and dispersibility of the nanomaterials. Additionally, it helps to increase the photocatalytic activity of the composite material, and can also decrease the electronic band gap energy, Furthermore, this method has been shown to improve the antimicrobial activity[6] of the nanocomposite, as well as the electrical conductivity. All of these properties make TiO_2 doped with PTA nanocomposites a promising material for various applications. The synergistic effect of TiO_2 and PTA creates a highly effective antibacterial agent, making these materials valuable for various medical applications, such as wound dressings, coatings for medical devices, and water disinfection systems. Another remarkable aspect of these nanocomposites is their enhanced electrical conductivity. PTA doping make charge carriers, thereby improving the electrical conductivity of TiO_2. This property opens up new possibilities for their application in energy storage and electronic devices[7].

One of the major research gaps in the field of TiO_2 nanocomposites is the understanding of the interactions between TiO_2 and the other materials in the nanocomposite. For example, it is important to understand how the other materials affect the band gap of TiO_2, which is a key factor in determining the photocatalytic activity of TiO_2. Further research is needed to optimize the synthesis and characterization of these composites, as well as to investigate their long-term stability and performance.

MATERIAL AND METHODS

For the synthesis of TiO_2 and TiO_2-Phosphotungstic acid nanocomposite, analytical grades reagents such as TiO_2, and PTA were used. All of these reagents were used according to standard laboratory procedures to ensure a successful synthesis.

Synthesis of TiO_2 doped with PTA nanocomposite

The Blending Method was an uncomplicated and simple technique for making nanocomposites. In the current study, sample preparation involved blending 1g of TiO_2 with the different concentrations of PTA for 60 minutes in a mortar. The blending process over, the blended composites were carefully placed in an air over at 110°C for 30 minutes and grinded the sample in a mortar. After, the four differing samples, namely sample 2, sample 3, sample 4, and sample 5 were prepared using the above grinding process with 0.01M, 0.001M, 0.05M, and 0.005M concentrations of PTA respectively.

Characterization Techniques

The Ultraviolet Visible diffuse reflectance spectra (UV-Vis DRS) of the samples were accurately measured by using the Jasco V-600 spectrophotometer for readings in the range of

200-900nm wavelength. In the analysis of Fourier transform infrared (FTIR) spectra, the Shimadzu 8400S model was used, while Jasco 550 double-beam spectrophotometer was efficiently utilized to capture the IR spectra. To gain further insights, in the PXRD (Powder X-ray diffraction) patterns of the products, an advanced Philips powder X-ray diffractometer (PW1710 Model) was operated at the rate of 2° min^{-1} utilizing Cu-Kα X-ray radiation as the source. This advanced diffractometer provided readings in the range of 10°-80° by taking steps of 0.02° and 1.25-sec interval step time, utilizing Copper Kα radiation (with wavelength of 1.5406 Å). The morphological information at the microscopic level was obtained by SEM (Scanning Electron Microscopes) with EDAX (Energy Dispersive X-ray Spectroscopy) and operated at the voltage of 20kV through the TESCAN VEGAS-3 model and ZEISS eco. This gives a detailed view of the samples that were analyzed to deduce their composition and structure, giving advanced insights into the material being studied.

The Kubelka–Munk function used the linear equation:

$$(\alpha hv)^2 \left(eVcm^{-1}\right)^2 \text{ vs Energy } (eV) \ldots\ldots\ldots\ldots\ldots\ldots (1)$$

where E represents the incident photon energy (hv) and α represents the absorption coefficient of the material. The linear plot of the Kubelka–Munk function helps in deciphering the position of band gap energy through visual inspection.

Urbach energy is an important parameter for the characterization of the material, as it affects its electrical and optical properties. It is usually measured by using the empirical equation.

$$ln\ \alpha = \frac{ln(C) - 1240}{hv} \ldots\ldots\ldots\ldots\ldots\ldots\ldots\ldots (2)$$

where lnα is the intensity of light, C is the concentration of the material, and hv is the energy of the incoming photon.

XRD pattern by Williamson Hall plot method

The d-spacing is calculated with the Bragg equation, which is defined as D=0.94λ/β*cosθ, where λ is the wavelength of the X-ray source, and θ is the Bragg angle of the peak. By plotting the peak intensity versus d-spacing, we can determine the crystallite size of the nanocomposite material.

$$D = \frac{0.94\lambda}{\beta cos\theta} \ldots\ldots\ldots\ldots\ldots\ldots\ldots (3)$$

The size of the particles in the sample can be determined from the Bragg's equation:

$$Size\ (nm) = \frac{0.94 \times \lambda}{(2 \times \beta \times cos\ \theta)} \ldots\ldots\ldots\ldots\ldots\ldots (4)$$

This equation considers two parameters. The first is d-spacing, which is the distance between two adjacent crystal planes, and is measured in nanometers. The second parameter is the diffraction angle (θ), and λ is X-ray wavelength.

The Williamson Hall plot was constructed by using the equation

$$\beta total \cos\theta = \varepsilon(4 \mathrm{Sin}\,\theta) + \frac{\kappa\lambda}{D} \ldots\ldots\ldots\ldots\ldots\ldots\ldots\ldots\ldots (5)$$

where βtotal is the full width at half maximum of a diffraction peak; θ is the Bragg angle; ε is the profile parameter; and kλ/(D) is the line broadening parameter, where k is a proportionality constant, λ is the X-ray wavelength and D is the grain size parameter.

Photocatalytic & Degradation activity

Photocatalytic experiments were conducted using inner photocatalytic reactor to degrade dye solutions. The photo reactor consist of borosilicate reactor tubes were placed in a reaction chamber. Subsequently, the solutions were exposed to ultraviolet radiation generated by the source of light having 365nm of wavelength, for a duration of three hours. In order to monitor the progress of the degradation of the dye, 2mL of samples of the dye solution were collected

at the time intervals of 10 minutes, 20 minutes, 30 minutes, 40 minutes, 50 minutes, 60 minutes, 120 minutes, and 180 minutes. The efficiency of degradation, an Optical Density (OD) spectrophotometer (Model 6300PC) was used to measure it at the wavelength of 460nm. The ratio between the initial concentration of Methylene Blue, denoted by 'C_o', and the corresponding concentration of the dye after a given amount of time 't' denoted by Ct were used to calculate the value of the percentage of degradation efficiency 'η'. The percentage of the degradation was computed according to the following equation:

$$\eta = \frac{(C_t - C_o)}{C_t \text{ X } 100} \ldots\ldots\ldots\ldots\ldots\ldots\ldots\ldots (6)$$

The objective of this experiment was to gain insight into the photodegradation behavior of photo catalyst and calculate the effectiveness of the photocatalytic process.

Electrical conductivity of TiO_2 based Nanocomposites

The electrical conductivity of pure TiO_2 and TiO_2-PTA composite, a powder sample was prepared by grinding the mixture of TiO_2 and TiO_2-PTA composite in a mortar. Moreover, 10 % weight of polyvinyl alcohol was also added as a binder to the powder, and the mixture was compressed into discs having a size of 11 mm in diameter and 3 mm in thickness, under the pressure of 260 MPa using a hydraulic press at room temperature. The result was a pellet of uniform shape and size. For obtaining the electrical conductivity of the samples, Two Probe method was used, which analyzed the frequency and temperature dependence of the electrical conductivity. An Agilent 4284A Precision LCR Meter was used for measuring the electrical conductivity with a temperature range of 303 to 393 K and a frequency range of 100 Hz to 1 MHz, in which each sample was placed between two blocking electrodes having a diameter of 2.5 cm, under a spring-like pressure. Two-probe method helps to measure both AC and DC conductive for a wide range of temperatures and frequencies. This makes it a reliable and ideal method for precisely measuring the electrical conductivity of TiO_2 and TiO_2-PTA nanocomposites.

The AC conductivity is determined by using the equation;

$$\varepsilon_r = \frac{2\pi Fcd}{A \tan \delta} \ldots\ldots\ldots\ldots (7)$$

The relative permittivity (ε_r) is measured by relating the applied frequency (F) to the dissipation factor or loss tangent (tan δ) to the electrode area (A) and the capacitance density (cd).

The dielectric constant is a measure of the intrinsic ability of a material to oppose changes in electric field strength, given as the ratio of capacitance (C) to the area (A) of the capacitor divided by permittivity of free space (ε_o). The dielectric constant is calculated by the following equation.

$$\varepsilon_r = \frac{cd}{A\varepsilon_o} \ldots\ldots\ldots\ldots (8)$$

The dielectric loss is explained by the equation.

$$\tan\delta = \frac{\varepsilon_r}{\varepsilon_o} \ldots\ldots (9)$$

where ε_r is the relative permittivity, and ε_o is the permittivity of free space. The ratio $\varepsilon_r/\varepsilon_o$ gives the ratio of the dielectric resistance to the resistance of a conductor in free space.

Antimicrobial activity of Nanocomposites

The Streptococcus pyogenes (MTCC 442) bacterial strain was obtained from HiMedia Laboratories Pvt. Ltd., Mumbai, India, grown in liquid Mueller Hinton Broth (M-H Broth) (HiMedia, Mumbai, India) at 33ºC for 2 hours with 200rpm stirring. The antimicrobial activity of TiO_2-doped with PTA nanocomposites was then evaluated utilizing the standard disk diffusion method. For the experiment, Nutrient Agar (NA) plates were separately daubed with bacterial suspensions of Streptococcus pyogenes using an L-rod. The process was also

facilitated by using Whatman filter paper (No.1) and discs of diameter 20 mm, which had been impregnated with a 20 µL solution of TiO_2-doped PTA nanocomposite in dimethyl sulfoxide (DMSO). Once the discs were air-dried, they were positioned on the agar plates. Amoxicillin and Potassium Clavulanate were incorporated as positive controls against bacteria and fungi respectively, each with a 20 µL solution of 20 mg/ml. Subsequently, the bacterial cultures were incubated at 37ºC and the fungus at 33ºC for 48 hours. Following this, the inhibitory diameter of the zone which indicated the activity zones of bacterial and nanocomposite growth, was measured and reported

RESULT AND DISCUSSION

UV-Vis spectra analysis

The UV-Vis spectra of Sample 1 (pure TiO_2) and Samples 2 to 5 TiO_2 doped with PTA nanocomposite (0.01M, 0.001M, 0.05M, and 0.005M of PTA) were given in figure 1 and table 1. In figure 1a, a broad peak was found in the ultraviolet range, and a sharp peak was found in the visible region for Sample 1 due to the bandgap of TiO_2. In samples 2 to 5 had a shift in the peak position and intensity compared to Sample 1, which can be associated with the incorporation of the dopants that can modify the optical properties of the TiO_2 composite. Significantly, the changes in the peak positions and intensities determined the concentration of the dopants. The results indicated that the optical properties of the nanocomposite changed with the addition of PTA as a dopant [8].

Optical Bandgap Energy

The optical band gap energy of sample 1 is 3.20eV while samples 2 to 5 are 2.79eV, 2.88eV, 2.90eV and 2.82eV respectively as shown in figure 2. The Tauc plot which is based on Kubelka–Munk function have been used to estimate the optical band gap energy of the materials.

In Tauc plot, the E from the Kubelka–Munk function is plotted against the incident photon energy (hv). As the incident photon energy of the material is increased, the absorption coefficient (α) of the material also increases, therefore displaying an increasing intercept on the y-axis (E) and a reduction in slope until the band gap energy is attained when the absorption coefficient (α) of the material becomes zero. The point at which the line intersects the y-axis and has a slope of zero is the estimation of the optical band gap energy of the material [9].

Optical Urbach Energy

Fig. 2. shows the Urbach energy of various samples. It is seen that the pure TiO_2 sample has an energy of 0.93 meV, while the doped TiO_2 samples have significantly lesser energy, ranging from 0.17 to 0.33 meV. The Urbach energy is a measurement of the energy width of the gap between the valence and conduction bands of a semiconductor material [10]. The Fig. 2. demonstrate that doping material, PTA significantly reduces its Urbach energy. The decrease in Urbach energy of the doped material has been shown in Fig.2 and in Table 1.

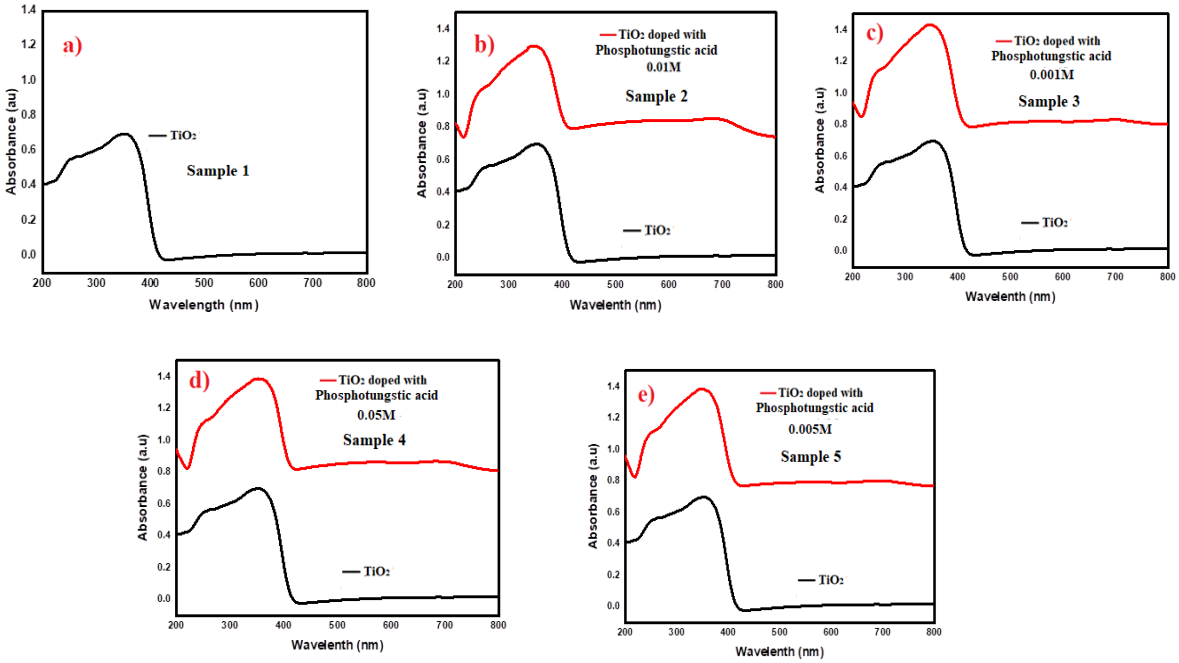

Figure 1. UV-Visible spectrum of (a) TiO_2 and (b to e) TiO_2-PTA nanocomposite.

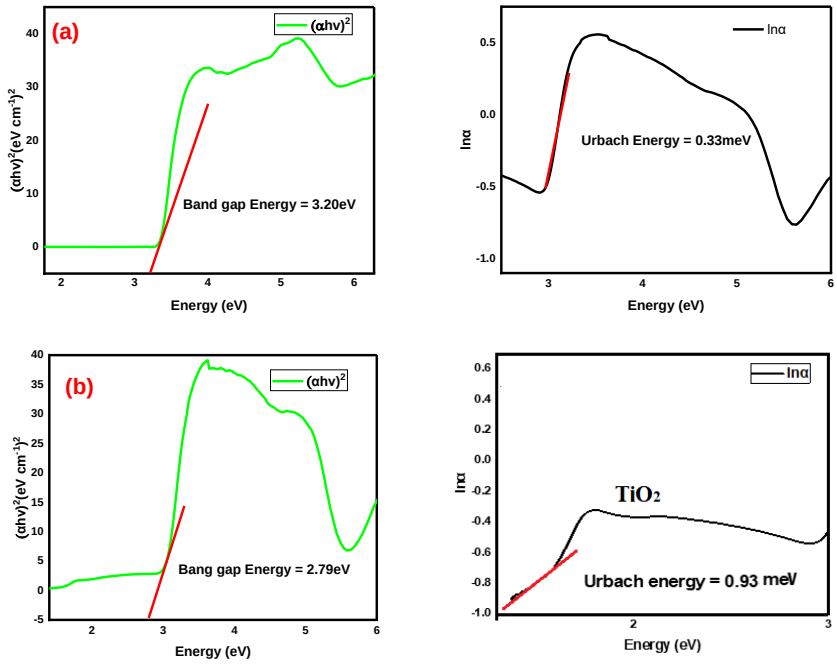

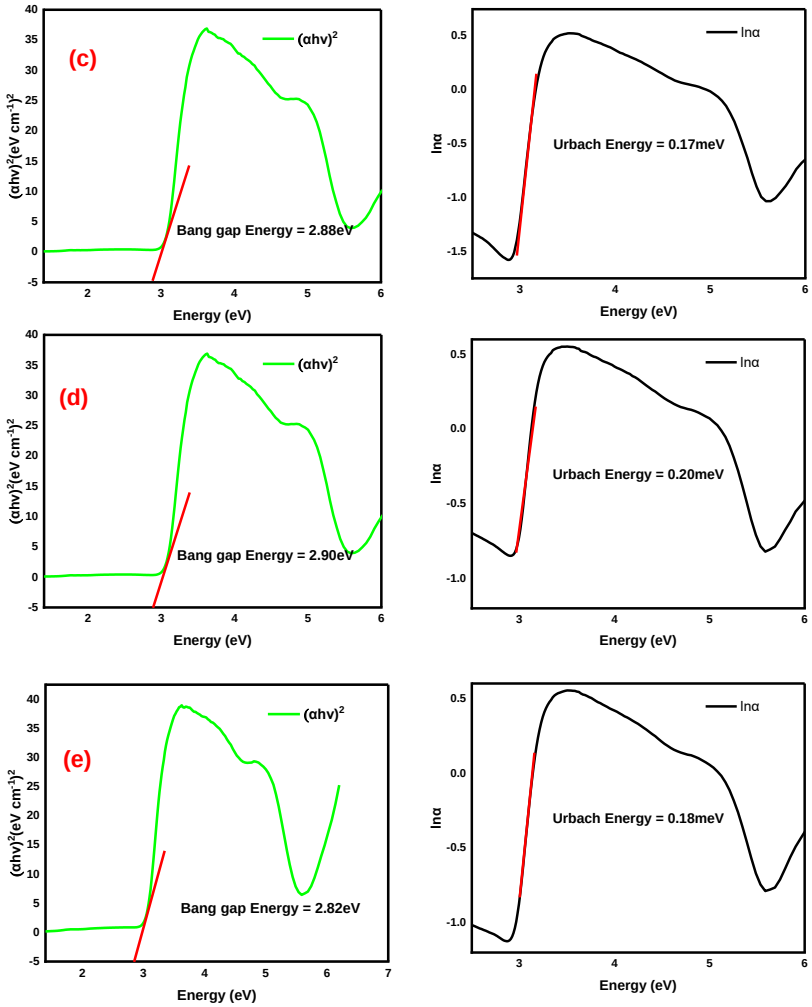

Fig.2. Band gap and Urbach energy of (a) TiO_2 and (b to e) TiO_2-PTA nanocomposite

Table 1. UV vis spectra, peaks, bandgap energy and Urbach energy.

Sample	UV-Vis peaks (nm)	Band gap Energy (eV)	Urbach Energy (meV)
TiO_2	350	3.20	0.93
Doped Sample (0.01M)	362	2.79	0.33
Doped Sample (0.001M)	356	2.88	0.17
Doped Sample (0.05M)	362	2.90	0.20
Doped Sample (0.005M)	358	2.82	0.18

FTIR Analysis

Figure 3 shows the FTIR spectra of sample 1. The spectrum shows four distinct peaks at 3420, 1379, 1007, and 625 cm^{-1}. frequencies range were recorded in 500-4000 cm^{-1}.

3420 cm^{-1} and 1379 cm^{-1} frequencies are characteristic of Ti-O stretching vibrations, while the 1007 cm^{-1} frequencies are characteristic of a Ti-O-Ti bending vibration. The 625 cm^{-1} frequency is also a Ti-O stretching vibration, but it is at a lower frequency than the other two frequencies. These Frequencies are characteristic of pure TiO_2, and their presence confirms the

identity of the sample.

The FTIR spectra of samples 2 to 5, TiO_2 doped with Phosphotungstic acid are shown in Figure 3. The spectra show a number of characteristic frequencies, which are summarized in Table 2. Sample 2 (0.01 M PTA) exhibits characteristic peaks at 3149, 1398, 1104, and 679 cm^{-1}. The frequencies at 3149 cm^{-1} are assigned to the stretching vibration of the Ti-O frequencies in TiO_2. The frequencies at 1398 cm^{-1} are assigned to the bending vibration of the Ti-O frequencies in TiO_2. The frequencies at 1104 cm^{-1} are assigned to the stretching vibration of the P=O frequencies in PTA. The frequencies at 679 cm^{-1} is assigned to the stretching vibration of the W=O Frequencies in PTA.

Sample 3 (0.001 M PTA) exhibits similar Frequencies to sample 2, but the intensities of the frequencies are lower. This suggests that the doping of TiO_2 with PTA is more effective at lower concentrations of PTA.

In Sample 4 the TiO_2 doped with 0.05 M PTA. The peaks at 3153, 1403, 1140, and 657 cm^{-1} are shifted to even higher wavenumbers than in sample 3. This indicates that the PTA doping has caused a more significant decrease in the frequency strengths in the TiO_2 lattice.

In Sample 5 the TiO_2 sample doped with 0.005 M PTA. The frequencies at 3145, 1398, 1135, and 696 cm^{-1} are intermediate between those in Samples 2 and 4. This indicates that the PTA doping has caused a moderate decrease in the frequency strengths in the TiO_2 lattice [11-12].

Overall, the FTIR spectra of the samples show that the PTA is having a significant effect on the structure of the TiO_2. This is due to the interaction between the PTA molecules and the TiO_2. The effect of the PTA is more pronounced at higher concentrations, but it is still present at lower concentrations.

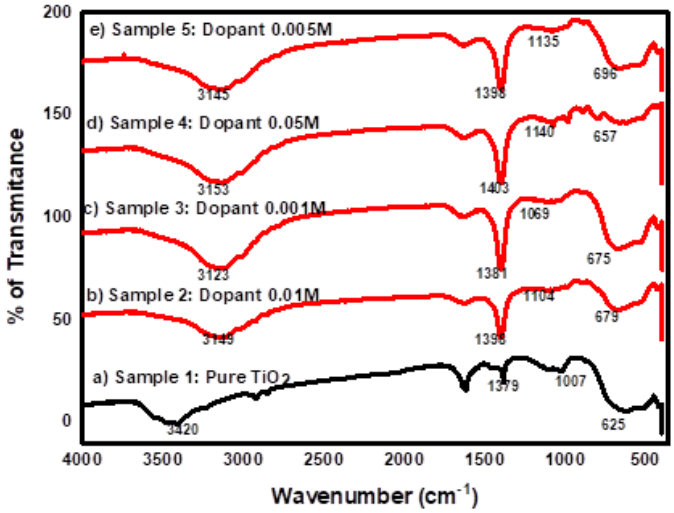

Figure 3. FTIR spectra of TiO_2-PTA nanocomposites.

PXRD Analysis

Figure 4 shows the PXRD analysis of sample 1, which was pure TiO_2. The JCPDS Card No. for this sample is 89-6975, and the crystal planes that were observed are (110), (004), (111), (210), (211), (220), (002), and (311). Samples 2-5 were TiO_2-Phosphotungstic acid (PTA) nanocomposites. The JCPDS Card No. for these samples are 76-1815, and the peaks were observed are (222), (400), (440), (511), (553), (642), and (800). These peaks correspond to the (h k l) values of the respective planes in the PTA composite [13].

The average crystallite size of the TiO_2 in sample 1 was calculated to be 29.63 nm using the Scherrer equation. Samples 2-5 were 37.35, 34.16, 35.49, and 37.68 nm, respectively. These results indicate that the doping of PTA into TiO_2 resulted in an increase in the average crystallite size.

The larger crystallite size in the doped samples are due to the presence of PTA, which is a

heteroatom dopant. Heteroatom doping can inhibit grain growth during the synthesis of TiO_2 nanoparticles, resulting in larger crystallite sizes.

The results of the PXRD analysis show that the doping of PTA into TiO_2 results in an increase in the average crystallite size. This increase in the average crystallite size is likely due to the formation of PTA-TiO_2 composites and the nucleation of TiO_2 crystals on the PTA molecules [14].

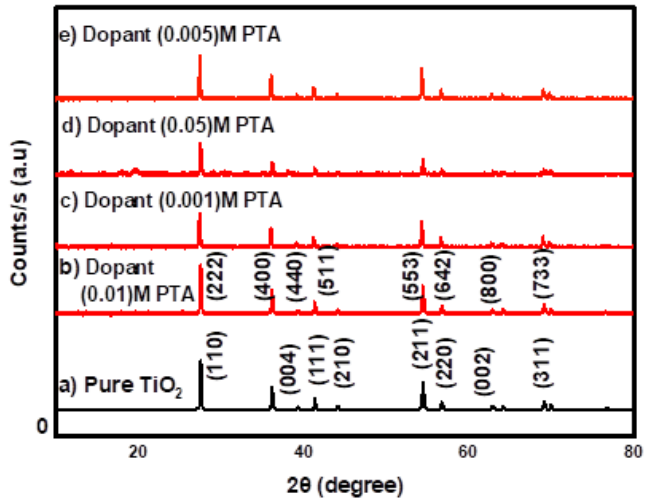

Fig.4. PXRD spectra of TiO_2 and TiO_2-PTA nanocomposites.

XRD pattern by Williamson Hall plot method

Fig. 5 shows the Williamson Hall plot for samples 1-5. From the graph, it can be observed that Sample 1 is pure TiO_2, while Samples 2 to 5 are doped with PTA. The graph is used to determine the crystallite size, d-spacing, FWHM, peak positions, intercepts, average crystallite size, slopes and micro strain as given in Table 2.

By plotting the peak intensity against the sinθ, the grain size and crystallite size are determined. The W-H plots for the TiO_2-PTA nanocomposites showed a linear relationship, as expected. The results of the XRD analysis provide valuable information about the structure and composition of the TiO_2-PTA nanocomposites. The results of this study suggest that the PTA doping can affect the particle size of TiO_2, and this could lead to new applications for these nanocomposites.[15].

Table 2. Williamson Hall plot using the XRD data

Nano composites	Peak Position 2θ (˚)	FWHM β (˚)	intercept c=kλ/D	Average Crystallite Size D(nm)	Slope m	Micro strain(ε) X10^{-3}	d-spacing (Å) d_{hkl}=λ/(2 sinθ)	Average d-spacing (Å)
TiO_2	27.14	0.2775	0.0037	29.63	0.0004	0.48	3.23	1.98
TiO_2 +PTA 0.01M	27.50	0.1775	0.0013	37.35	0.0014	1.48	3.41	2.47

TiO_2 +PTA 0.001M	27.36	0.2167	0.0028	34.16	0.0008	0.85	3.25	1.99
TiO_2 +PTA 0.05M	17.87	0.3531	0.0004	35.49	0.0020	2.07	4.95	2.82
TiO_2 +PTA 0.005M	27.38	0.1895	0.0002	37.68	0.0007	0.77	3.25	1.98

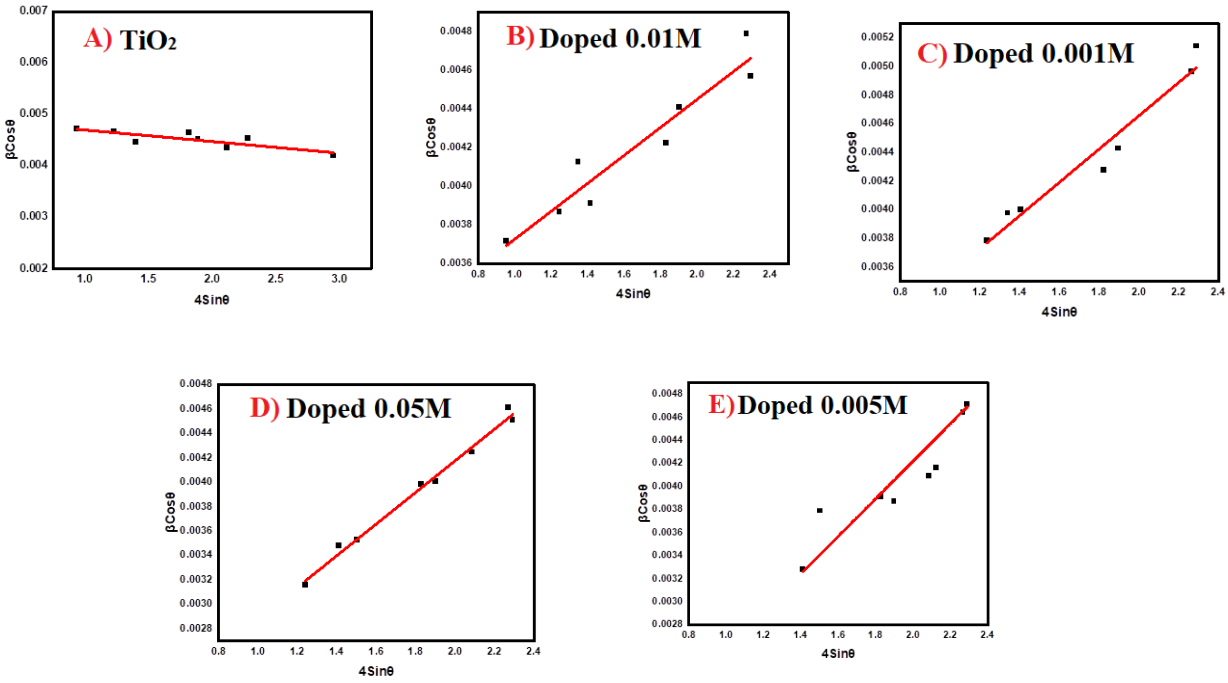

Fig.5. W-H spectra of TiO_2 and TiO_2-PTA composites.

SEM with EDAX analysis

Figure 6 shows SEM with EDAX analysis of sample 1 and samples 2–5 nanocomposites. SEM images show that the particles in sample 1 is relatively smooth and uniform in size. For sample 2-5 as the concentration of phosphotungstic acid increases, the particles become more rough and irregular in shape. This is likely due to the fact that the phosphotungstic acid interfere with the crystal growth of the TiO_2 particles [16].

The EDAX analysis shows that the major elements in all samples are oxygen and titanium. The doped samples also contain phosphorus and tungsten. The amount of phosphorus and tungsten increases with increasing concentration of the PTA nanocomposite. The EDAX analysis shows that the pure TiO_2 sample is composed of 66% TiO_2 and 34% oxygen. The doped samples also contain PTA, with the concentration of PTA increasing with increasing doping concentration. For example, the 0.01M doped sample contains 11% PTA, the 0.001M doped sample contains 4% PTA, the 0.05M doped sample contains 4.85% PTA.

The results of the SEM and EDAX analysis suggest that the doping of TiO_2 with PTA can increase the size of the particles and the amount of phosphorus and tungsten in the particles. These results suggest that the PTA nanocomposites are well-dispersed in the TiO_2 matrix, and

that they do not significantly affect the morphology or composition of the particles [17].

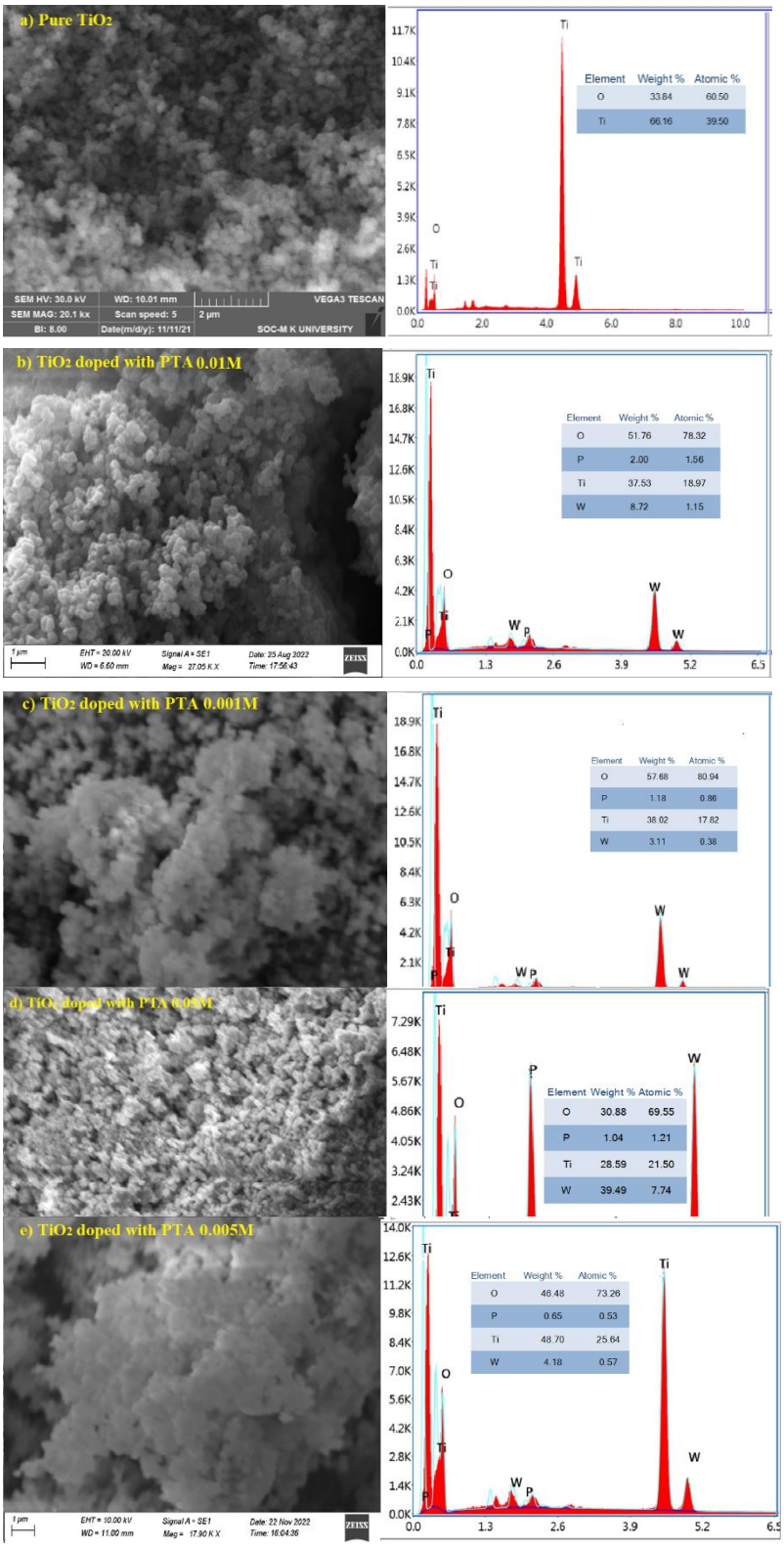

Fig.6. SEM with EDAX Analysis of (a) TiO_2 and (b to e) TiO_2-PTA nanocomposites

Color mapping analysis

Figure 7 shows a SEM image of a TiO_2 doped with phosphotungstic acid. The images are color mapping to show the different elements in the nanocomposites. The yellow areas represent titanium (Ti), the blue areas represent oxygen (O), the violet areas represent phosphorus (P), and the red areas represent tungsten (W).

The image shows that the nanocomposites composed of a heterogeneous mixture of Ti, O, P, and W. The Ti atoms are clustered together in small, spherical particles. The O atoms are distributed more evenly throughout the nanocomposite. The P and W atoms are present in smaller amounts, and they are also distributed more evenly throughout the nanocomposite.

The composition of the nanocomposite is consistent with the elemental analysis results, which showed that the nanocomposite is composed of 49% Ti, 31% O, 6% P, and 14% W. The results of SEM and elemental analysis confirm that the nanocomposite was successfully synthesized [18-19]

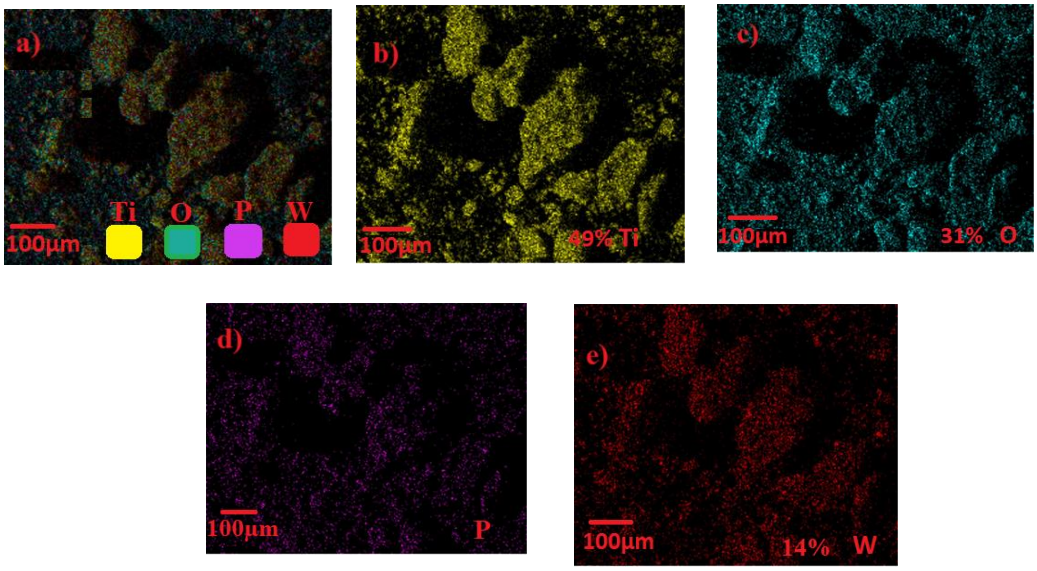

Fig.7. Color mapping Analysis of TiO_2 and TiO_2-PTA nanocomposites.

Average particle analysis

Figure 8 shows an SEM image of TiO_2 composites using ImageJ software. The image shows the average particle size of sample 1 is 0.15 nm. The particle size was found to increase with increasing concentration, with the largest particles being observed at the highest concentration (0.05 M). The average particle sizes for the different concentrations 0.01, 0.001, 0.05, and 0.005 M were 19.43, 16.81, 14.58, and 5.47 nm respectively. The histogram shows that the majority of the particles in the sample are small, with a few larger particles. The increase in particle size with increasing concentration is likely due to the aggregation of particles. At lower concentrations, the particles are more dispersed and have a smaller average size. However, as the concentration increases, the particles have more opportunity to collide and aggregate, resulting in larger particles. The results of this study show that the particle size of TiO_2 can be controlled by adjusting the concentration of the PTA [20]. This could be useful for applications where the particle size of TiO_2 is important, such as photocatalysis and optical devices. Overall, this study provides new insights into the effect of concentration on the particle size and shape of TiO_2 nanocomposites. These findings could be useful for the development of new TiO_2-based materials with enhanced properties.

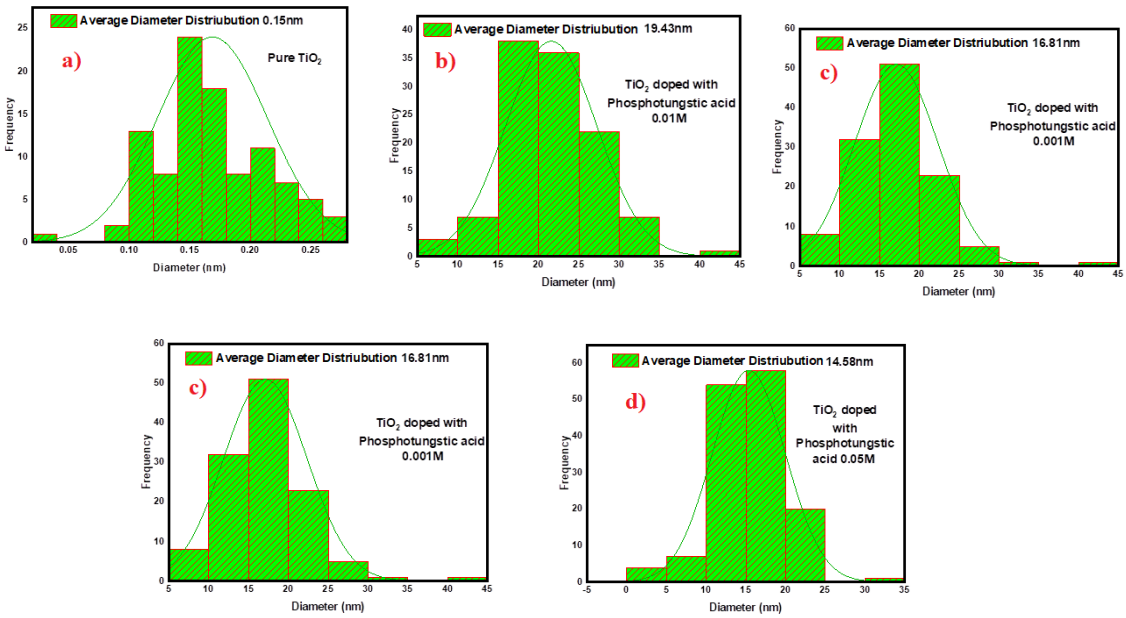

Fig.8. Average diameter distribution Analysis of TiO_2 and TiO_2-PTA nanocomposites.

Photocatalytic Studies

Photodegradation studies of methylene blue dye by TiO_2-PTA composite without air flow

The photodegradation of methylene blue in the presence of TiO_2-PTA catalyst was measured under the following conditions: methylene blue concentration 50 ppm, temperature (33^{o}C), photodegradation wavelength (365nm) and for degraded samples optical density (OD) measured at λmax =460nm. These experiments were conducted without airflow. Six different TiO_2-PTA catalyst concentrations were investigated, such as 10mg, 20mg, 50mg, 100mg, 125mg, and 150mg/L.

The results of the study indicate that the highest level of methylene blue degradation occurred when the TiO_2-PTA catalyst concentration at 150mg/L and the highest degradation (84.01%) was achieved. At the lower photocatalyst concentrations (10mg and 20mg), the methylene blue degradation are found to be 9% and 15%, respectively.

The degradation rates at other concentrations 50mg, 100mg, and 125mg are 49%, 75%, and 88%, respectively. Overall, the study demonstrates that increasing the TiO_2-PTA catalyst concentration is effective in improving the methylene blue

photodegradation efficiency up to 150mg and then decreases. The results of this study showed that the photocatalytic degradation efficiency of methylene blue increased with

increasing catalyst concentration. The optimum catalyst concentration for the photocatalytic degradation of methylene blue was found to be 150 mg. These results suggest that PTA is a promising photocatalyst for the degradation of methylene blue. At low catalyst concentrations, the number of active sites on the catalyst surface is limited. However, as the catalyst concentration is increased, the number of active sites on the surface increases, which leads to an increase in the photocatalytic activity [21-22].

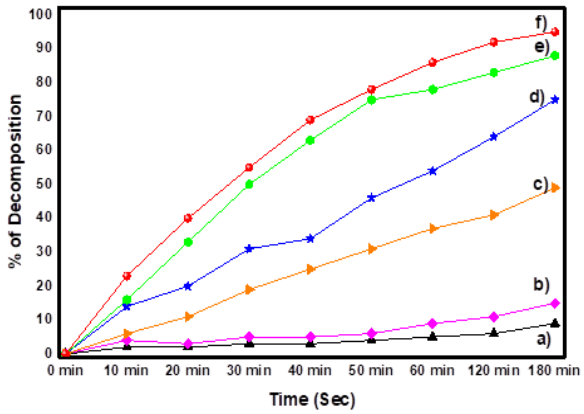

Fig.10. PTA photocatalyst concentration variation.
a) 10mg b) 20mg c) 50mg d) 100mg e) 125mg f) 150mg
Condition**:** Methylene blue = 50mg/L; Temp = 33ºC; Without airflow and Photodegradation wavelength = 365nm, and O.D measured at λ_{max}= 460 nm

Effect of pH on photocatalytic degradation of methylene blue

The effects of various pH levels on photocatalytic degradation of methylene blue were investigated. A solution of 50mg/L methylene blue is mixed with 0.5g/L of a catalyst and exposed to UV radiation at 365nm with an absorbance of 460nm. The pH of the solution is then adjusted to readings of 4, 6, and 8 using 0.1M HCl and NaOH. After a period of 60 minutes, the degradation efficiencies are recorded at 64.50%, 56.39%, and 38.76%, for pH levels of 4, 6, and 8 respectively. The highest degradation occurred at pH 4, and the lowest at pH 6 and 8, likely because, the availability of the methylene blue's aromatic ring was decreased at higher pHs, resulting in lesser degradation efficiency. The results of this study suggest that the pH of the solution is an important factor to consider when using photocatalysis to degrade methylene blue. In order to achieve the highest degradation efficiency, the pH of the solution should be adjusted to be slightly acidic [23].

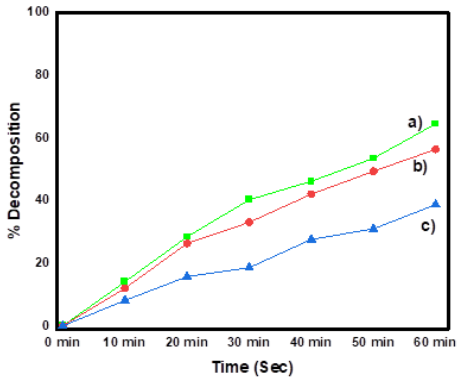

Fig. 11. Effect of pH variation on photodegradation of methylene blue
a) 4 b) 6 c) 8
Condition: Methylene blue = 50mg/L; Temp = 33ºC; catalyst dose = 0.5g/L
Photodegradation wavelength = 365nm,

Effect of demineralization of Methylene blue dye

Figure 12. shows the effect of demineralization of methylene blue dye under different conditions. The dye degraded at a concentration of 50mg/L, and the temperature was 33ºC. The catalyst dose was 0.5g/L, and the photodegradation wavelength was 365nm. The demineralization was complete at different times, depending on the conditions.

The demineralization of methylene blue dye is a time-dependent process. After 1 hour, the demineralization is 64.42%, and it increases to 78.3% after 2 hours. After 3 hours, the demineralization is 90.23%, and it reaches 95.23% after 4 hours. After 5 hours, the demineralization is 99.56%, and complete demineralization (100%) occurs after 6 hours. The results of this study could be useful for the development of methods for the removal of methylene blue dye from wastewater or other environmental matrices. Moreover, this demineralization process provides an effective way to remove the dye from wastewater before it enters the environment. The main advantage of the process is that the dye can be removed from the water without any residues [24].

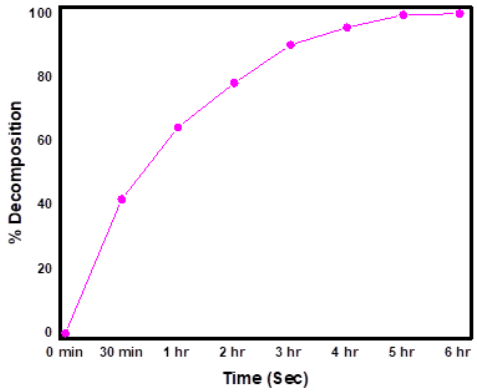

Fig. 12. Effect of demineralization of Methylene blue dye
Condition: Methylene blue = 50mg/L; Temp = 33ºC; catalyst dose = 0.5g/L and Photodegradation wavelength = 365nm

Electrical conductivity studies by Two probe method

TiO_2-PTA nanocomposites (0.05M of PTA) was investigated in this study. The results showed that PTA can significantly improve the electrical conductivity of the material. The conductivity of the doped sample was higher than that of the pure TiO_2 sample. Additionally, the conductivity of the doped sample increased when the frequency was increased from 100 Hz to 1 MHz, indicating a frequency-dependent response. This is attributed to the doping of the TiO_2 with the phosphorus-tungsten heteropoly acid, which acts as an electron donor, increasing the number of available charge carriers and the electrical conductivity [25].

AC and DC conductivity studies were conducted to investigate the electrical properties of the doped TiO_2 samples. The AC conductivity measurements showed that the doped samples had a higher conductivity than the pure TiO_2 sample at all frequencies. The DC conductivity measurements showed that the doped samples also had a higher conductivity than the pure TiO_2 sample, but the difference was more pronounced at higher frequencies.

The results of this study suggest that PTA doping can be a promising strategy for improving the electrical conductivity of TiO_2.

AC conductivity Studies of TiO_2 and TiO_2-PTA Composite

Figure 13 shows the electrical conductivity studies of TiO_2 and TiO_2-PTA nanocomposite by using the two-probe method. The conductivity of pure TiO_2 were increasing with temperature in the range of 303-393 K. The conductivity of TiO_2-PTA nanocomposite also increases with

temperature at 303 K, but it decreases at 333-393 K. The overall frequency range is from 100 to 200,000 Hz.

The increase in conductivity with temperature is due to the increased mobility of the charge carriers. As the temperature increases, the thermal energy of the charge carriers increases, which allows them to more easily overcome the energy barriers that prevent them from moving. For TiO_2-PTA nanocomposites, the conductivity at 303 K increases with increasing frequency, but the conductivity at 333, 363, and 393 K decreases with increasing frequency. In TiO_2-PTA nanocomposite, the conduction is also dominated, but the PTA dopants also create new conduction pathways. These pathways are more efficient at conducting electrons, leading to an even greater increase in conductivity at low temperatures. However, at higher temperatures, the PTA dopants begin to scatter the electrons, leading to a decrease in conductivity [26].

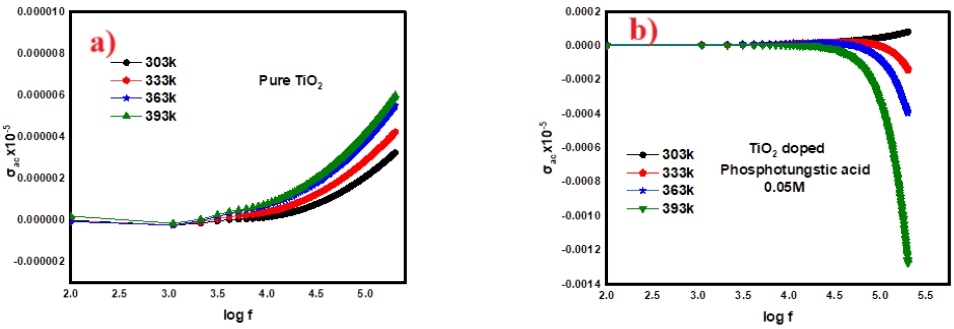

Fig.13. Frequency-dependent AC conductivity of Pure TiO_2 and TiO_2-PTA nanocomposites at varying temperatures

DC conductivity Studies of TiO_2 and TiO_2-PTA Composite

Figure 14 shows the electrical conductivity studies of pure TiO_2 and TiO_2-PTA nanocomposite, at a temperature of 33 °C and voltage ranges from 0 to 400 volts. The graph shows that the electrical conductivity of both materials increases linearly with voltage, but the conductivity of TiO_2-PTA is significantly higher than that of pure TiO_2.

This is because the doping of TiO_2 with PTA introduces additional carriers into the material, which increases its conductivity. The PTA molecules act as electron donors, which can donate electrons to the TiO_2 lattice. This creates more free electrons in the material, which increases its ability to conduct electricity.

The results of this study show that the electrical conductivity of TiO_2 can be significantly increased by doping it with PTA. This makes TiO_2-PTA a promising material for applications [27].

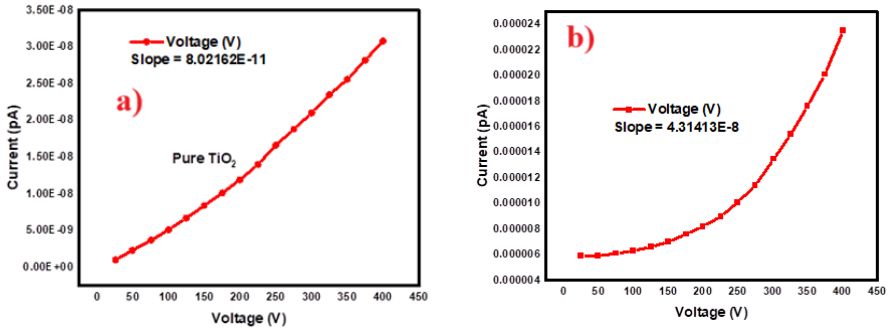

Fig. 14. DC Conductivity of Pure TiO_2 and TiO_2-PTA nanocomposite

Dielectric studies of TiO_2 and TiO_2-PTA Composite

Figure 15 shows the dielectric constant studies of pure TiO_2 and TiO_2 doped with PTA (0.05M

of PTA), at temperature ranges of 303, 333, 363, and 393 K. The dielectric constant of pure TiO_2 is significantly reduced when PTA is added. This is because the PTA molecules disrupt the regular arrangement of the TiO_2 atoms, which reduces the polarizability of the material. As can be seen in the figure, the dielectric constant of both sample is significantly reduced at all four temperatures.

This is because the thermal energy of the electrons increases with temperature, which makes it easier for them to move around and polarize the material. TiO_2 is significantly reduced when it is doped with PTA. PTA is a polar molecule, which can polarize the surrounding TiO_2 ions. The reduction in the dielectric constant of TiO_2 when PTA is added is beneficial for some applications. For example, in capacitors, a lower dielectric constant means that the capacitor can store more charge for a given voltage. This makes PTA-doped TiO_2 a promising material for use in high-density capacitors.

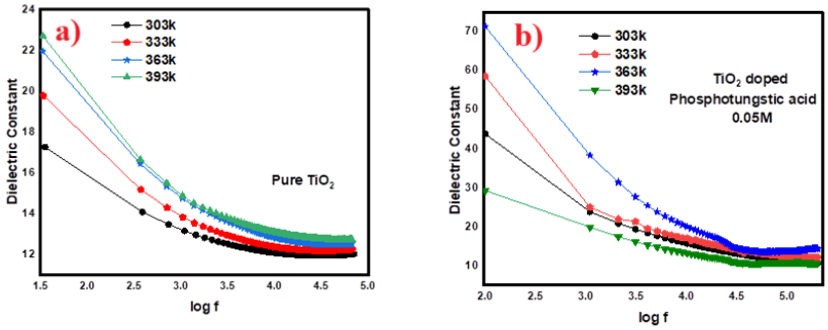

Fig. 15. Frequency dependent dielectric constant for Pure TiO_2 and TiO_2-PTA nanocomposites at varying temperatures

Figure 16 shows the dielectric loss of pure TiO_2, and TiO_2 doped with PTA nanocomposites (0.05M), at temperature ranges of 303, 333, 363, and 393 K. The results show that the dielectric loss of the PTA-doped TiO_2 nanocomposites is significantly lower than that of pure TiO_2 at all temperatures and frequencies. This is due to the fact that the PTA molecules act as a barrier to the movement of charge carriers, which reduces the dielectric loss.

The graph of ε_r vs. log f(Hz) shows that the dielectric constant of the PTA-doped TiO_2 nanocomposites decreases with increasing frequency. This is due to the fact that the PTA molecules become less effective at blocking the movement of charge carriers at higher frequencies. This is because the dielectric loss and AC conductivity are inversely proportional. The reduced losses is attributed to the improved surface morphology of the TiO_2 nanocomposite due to the strong interaction between PTA and TiO_2 particles, as well as the increased amount of electrical charges due to the chemical reaction between TiO_2 and PTA [28]. Overall, the results of this study show that the addition of PTA to TiO_2 can significantly reduce the dielectric loss and increase the AC conductivity of the resulting nanocomposites. This makes them promising materials for a variety of applications, such as dielectric capacitors and sensors.

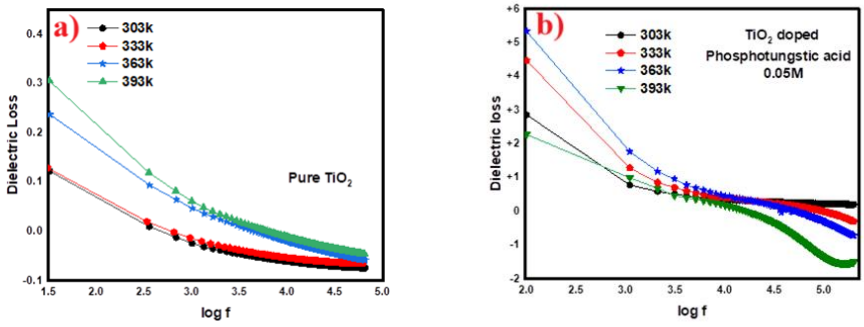

Fig. 16. Frequency dependent dielectric loss for Pure TiO_2 and TiO_2-PTA nanocomposites at

varying temperatures

Antimicrobial activity by Disc diffusion method

Figure 17 shows the antimicrobial activity of TiO_2 doped with PTA (0.05 M) dissolved in dimethyl sulfoxide (DMSO) solution was evaluated using the disk diffusion method on nutrient agar medium. Streptococcus pyogenes bacteria was used as the test organism and the antibiotic amoxicillin potassium clavulanate was used as the control. On the nutrient agar medium, 20 µl TiO_2 doped with PTA (0.05 M) and 20 µl of the control antibiotic amoxicillin potassium clavulanate were loaded onto blank filter paper disks. Control 1 was TiO_2 doped with PTA and Control 2 was antibiotic amoxicillin potassium clavulanate. The filter paper disks were cut into 5 mm diameter rings using a L-rod. The rings were placed onto the medium and after 48 hours of incubation at 37 °C, the zone of inhibition was measured.

The results showed that TiO_2 doped with PTA had significant antimicrobial activity against Streptococcus pyogenes. The zone of inhibition of TiO_2 doped with PTA was significantly greater than that of the antibiotic amoxicillin potassium clavulanate. The antibacterial activity of the TiO_2 doped with PTA nanocomposite was found to be greater than that of the control antibiotic, indicating it could be a superior antimicrobial agent[29-30].

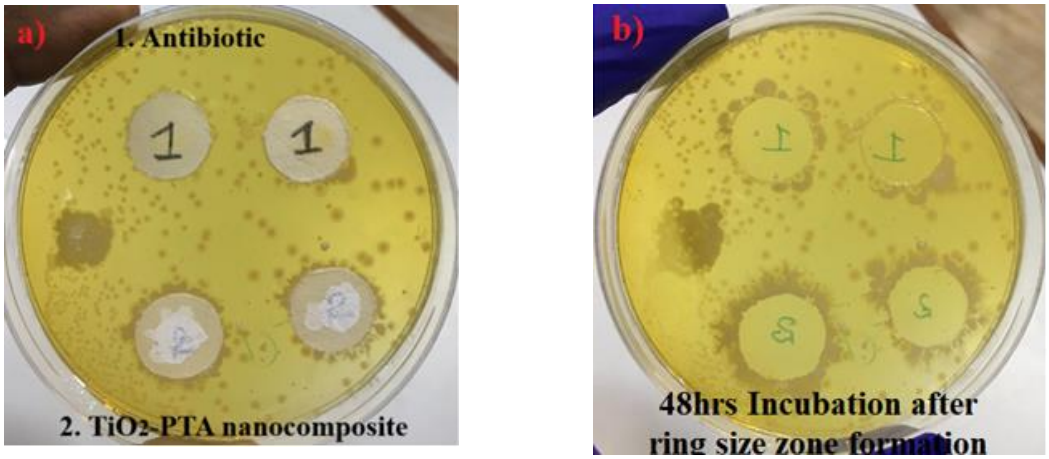

Fig. 17. Antimycobacterial activity TiO_2 doped PTA nanocomposites

Conclusion

The key findings of this study has shown that TiO_2 doped with PTA can be synthesized by blending method and characterized by UV-vis, FTIR, XRD, SEM and EDX. The results showed that there was a strong interaction between TiO_2 and PTA, which resulted in a shift in peak position, decreases of crystallinity, decreases of particle size and uniform distribution of dopant into the TiO_2 matrix.

In photocatalysis, the preliminary experiment confirmed the essential of light and catalyst for the degradation of methylene blue. The established optimal condition was at pH=4 with [Methylene blue] =50ppm; temperature=33ºC, catalyst dose=0.05M; without airflow and photodegradation wavelength =365nm under this condition, TiO_2-PTA exhibited the maximum efficiency (95%).

The disc diffusion method showed that TiO_2-PTA composite
combined with amoxicillin potassium clavulanate, demonstrated a potent antimicrobial effect against streptococcus pyogenes bacteria. This makes it a promising treatment option for infection caused by this particular bacterial.

Furthermore, it was observed that the TiO_2-PTA composite exhibited AC and DC conductivities, which increases with increase in temperature and frequencies.

Overall, this study has shown that TiO_2 doped with PTA is a promising material for photocatalysis, electrical and antimicrobial applications.

ACKNOWLEDGMENTS

I would like to thank faculty of the Department of Chemistry & Zoology, St. John's College, Palayamkottai. For providing necessary facilities to conduct the experiments.

Conflicts of interest

The authors declare no conflicts of interest

REFERENCES:

i. Pourmadadi M.; Rajabzadeh-Khosroshahi, M.; Eshaghi, M. M.; Rahmani, E.; Motasadizadeh, H.; Arshad, R.; Rahdar, A.; Pandey, S. TiO_2-Based Nanocomposites for Cancer Diagnosis and Therapy: A Comprehensive Review. Journal of Drug Delivery Science and Technology 2023, **82**, 104370.

ii. Kaur A.; Kaur, M.; Singh, V.; Vyas, P. Nanocomposites of Ferrites with TiO_2, SiO_2 and Carbon Quantum Dots as Photocatalysts for Degradation of Organic Pollutants and Microbes. Magnetochemistry 2023, **9** (5), 127.

iii. Hassan T.; Salam, A.; Khan, A.; Khan, S. U.; Khanzada, H.; Wasim, M.; Khan, M. Q.; Kim, I. S. Functional Nanocomposites and Their Potential Applications: A Review. J Polym Res 2021, **28** (2), 36.

iv. Liu K.-G.; Sharifzadeh, Z.; Rouhani, F.; Ghorbanloo, M.; Morsali, A. Metal-Organic Framework Composites as Green/Sustainable Catalysts. Coordination Chemistry Reviews 2021, **436**, 213827.

v. Wu J.; Wu, D.; Peng, W.; Ji, Y.; Tong, H. Research Progress of Polyoxometalates Photocatalyst for Degradation of Organic Wastewater. ACE 2022, **5** (1), 92.

vi. Torkian N.; Bahrami, A.; Hosseini-Abari, A.; Momeni, M. M.; Abdolkarimi-Mahabadi, M.; Bayat, A.; Hajipour, P.; Amini Rourani, H.; Abbasi, M. S.; Torkian, S.; Wen, Y.; Yazdan Mehr, M.; Hojjati-Najafabadi, A. Synthesis and Characterization of Ag-Ion-Exchanged Zeolite/TiO_2 Nanocomposites for Antibacterial Applications and Photocatalytic Degradation of Antibiotics. Environmental Research 2022, **207**, 112157.

vii. Alshehri E. M.; Alarfaj, N. A.; Al-Tamimi, S. A.; El-Tohamy, M. F. Electroanalytical Sensors-Based Biogenic Synthesized Metal Oxide Nanoparticles for Potentiometric Assay of Pantoprazole Sodium. Green Chemistry Letters and Reviews 2023, **16** (1), 2240837.

viii. Subudhi S.; Tripathy, S. P.; Parida, K. Highlights of the Characterization Techniques on Inorganic, Organic (Cof) and Hybrid (Mof) Photocatalytic Semiconductors. Catal. Sci. Technol. 2021, **11** (2), 392–415.

ix. Lai S. Y.; Ng, K. H.; Cheng, C. K.; Nur, H.; Nurhadi, M.; Arumugam, M. Photocatalytic Remediation of Organic Waste over Keggin-Based Polyoxometalate Materials: A Review. Chemosphere 2021, **263**, 128244.

x. Sharma T.; Garg, M. Pristine, Irradiated and Nanocomposite Polystyrene: Recent Experimental and Theoretical Developments. Trans. Electr. Electron. Mater. 2021, **22** (4), 394–418.

xi. Lakshmi M. S.; Wabaidur, S. M.; Alothman, Z. A.; Johan, M. R.; Ponnusamy, V. K.; Dhanusuraman, R. Phosphotungstic ACID-TITANIA Loaded Polyaniline Nanocomposite as Efficient Methanol ELECTRO-OXIDATION Catalyst in Fuel Cells. Int J Energy Res 2021, **45** (6), 8243–8254.

xii. Akbari Beni F.; Gholami, A.; Ayati, A.; Niknam Shahrak, M.; Sillanpää, M. UV-Switchable Phosphotungstic Acid Sandwiched between ZIF-8 and Au Nanoparticles to Improve Simultaneous Adsorption and UV Light Photocatalysis toward Tetracycline Degradation. Microporous and Mesoporous Materials 2020, **303**, 110275.

xiii. Lin Z.; Huang, J. A Hierarchical $H_3PW_{12}O_{40}/TiO_2$ Nanocomposite with Cellulose as Scaffold for Photocatalytic Degradation of Organic Pollutants. Separation and Purification Technology 2021, **264**, 118427.

xiv. Hassan S. M.; Ahmed, A. I.; Mannaa, M. A. Surface Acidity, Catalytic and Photocatalytic Activities of New Type $H_3PW_{12}O_{40}$/Sn-TiO_2 Nanoparticles. Colloids and Surfaces A: Physicochemical and Engineering Aspects 2019, **577**, 147–157.

xv. Habibi Jetani G.; Rahmani, M. B. TiO_2/GO Nanocomposites: Synthesis, Characterization, and DSSC Application. Eur. Phys. J. Plus 2020, **135** (9), 720.

xvi. Sanjaya A. R.; Atan, D. P.; Putra, G. A. M.; Setiyo Widodo, D. Titanium Dioxide Effect on the Decolourisation of Organic Dyes Remazol Black B Using Electrocoagulation in Situ -Fe_2O_3. International Journal of Environmental Analytical Chemistry 2023, 1–16.

xvii. Safari J.; Tavakoli, M.; Ghasemzadeh, M. A. A Highly Effective Synthesis of Pyrimido[4,5-b] Quinoline-Tetraones Using $H_3PW_{12}O_{40}$/Chitosan/$NiCo_2O_4$ as a Novel Magnetic Nanocomposite. Polyhedron 2020, **182**, 114459.

xviii. Bharat N.; Bose, P. Influence of Nano-TiO_2 Particles on the Microstructure, Mechanical and Wear Behaviour of AA7178 Alloy Matrix Fabricated by Stir Casting Technique. Proceedings of the Institution of Mechanical Engineers, Part L: Journal of Materials: Design and Applications 2023, **237** (4), 753–766.

xix. Suppuraj P.; Thirunarayanan, G.; Rajalakshmi, S.; Usha, V.; Sundaramurthy, N.; Swaminathan, M.; Muthuvel, I. $TiO_2/ZnFe_2O_4$ Nanospheres: An Efficient, Photocatalytic, Electrocatalytic and Cytotoxicity Applications. Materials Today: Proceedings 2021, **43**, 2134–2139.

xx. Haghighatzadeh A.; Hosseini, M.; Mazinani, B.; Shokouhimehr, M. Improved Photocatalytic Activity of ZnO-TiO_2 Nanocomposite Catalysts by Modulating TiO_2 Thickness. Mater. Res. Express 2019, **6** (11), 115060.

xxi. N, R.; anwar; Bamne, J.; Singh, N.; Sharma, P. K.; Singh, P.; Umar, A.; Haque, F. Z. Synthesis of Titania/Silica Nanocomposite for Enhanced Photodegradation of Methylene Blue and Methyl Orange Dyes under Uv and Mercury Lights. ES Materials & Manufacturing 2022, Volume 16 (June 2022) (0), 78–88.

xxii. Mahamud M.; Taddesse, A. M.; Bogale, Y.; Bezu, Z. Zeolite Supported CdS/TiO_2/CeO_2 Composite: Synthesis, Characterization and Photocatalytic Activity for Methylene Blue Dye Degradation. Materials Research Bulletin 2023, **161**, 112176.

xxiii. Bhapkar A.; Prasad, R.; Jaspal, D.; Shirolkar, M.; Gheisari, Kh.; Bhame, S. Visible Light Driven Photocatalytic Degradation of Methylene Blue by ZnO Nanostructures Synthesized by Glycine Nitrate Auto Combustion Route. Inorganic Chemistry Communications 2023, **148**, 110311.

xxiv. Manea Y. K.; Khan, A. M.; Wani, A. A.; Saleh, M. A. S.; Qashqoosh, M. T. A.; Shahadat, M.; Rezakazemi, M. In-Grown Flower like Al-Li/Th-LDH@CNT Nanocomposite for Enhanced Photocatalytic Degradation of MG Dye and Selective Adsorption of Cr (Vi). Journal of Environmental Chemical Engineering 2022, **10** (1), 106848.

xxv. Sebak M. A.; Qahtan, T. F.; Asnag, G. M.; Abdallah, E. M. The Role of TiO_2 Nanoparticles in the Structural, Thermal and Electrical Properties and Antibacterial Activity of Peo/Pvp Blend for Energy Storage and Antimicrobial Application. J Inorg Organomet Polym 2022, **32** (12), 4715–4728.

xxvi. Parvathi K.; Ramesan, M. T. Effect of Titanium Dioxide on the Structural, Thermal, and Electrical Properties of Chlorinated Natural Rubber/Poly (Indole) Blend Nanocomposites for Flexible Nanoelectronic Devices. J of Applied Polymer Sci 2023, **140** (11), e53621.

xxvii. Mahmoud Z. H.; AL-Bayati, R. A.; Khadom, A. A. In Situ Polymerization of Polyaniline/Samarium Oxide-Anatase Titanium Dioxide (PANI/Sm_2O_3-TiO_2) Nanocomposite: Structure, Thermal and Dielectric Constant Supercapacitor Application Study. J. Oleo Sci. 2022, **71** (2), 311–319.

xviii. Rajesh K.; Crasta, V.; Rithin Kumar, N. B.; Shetty, G.; Rekha, P. D. Structural, Optical, Mechanical and Dielectric Properties of Titanium Dioxide Doped PVA/PVP Nanocomposite. J Polym Res 2019, **26** (4), 99.

xxix. Deshmukh S. P.; Koli, V. B.; Dhodamani, A. G.; Patil, S. M.; Ghodake, V. S.; Delekar, S. D. Ultrasonochemically Modified Ag@TiO_2 Nanocomposites as Potent Antibacterial Agent in the Paint Formulation for Surface Disinfection. ChemistrySelect 2021, **6** (1), 113–122.

xxx. Mariselvi P.; Kumar, T. A. Antibacterial Activities of Calcareous/TiO_2 Nanocomposites. JPRI 2021, 377–388.

Received on September 5, 2023.